Applied Mathematical Modelling 46 (2017) 674–690

Contents lists available at ScienceDirect

Applied Mathematical Modelling

journal homepage: www.elsevier.com/locate/apm

A study on torsional vibration attenuation in automotive drivetrains using absorbers with smooth and non-smooth nonlinearities

Ahmed Haris[a], Eliot Motato[a], Stephanos Theodossiades[a,*], Homer Rahnejat[a], Patrick Kelly[b], Alexander Vakakis[c], Lawrence A Bergman[d], D. Michael McFarland[d]

[a] Wolfson School of Mechanical, Electrical and Manufacturing Engineering, Loughborough University, Loughborough LE11 3TU, United Kingdom
[b] Ford Werke GmbH, Cologne, Germany
[c] Department of Mechanical Science and Engineering, University of Illinois Urbana-Champaign, Urbana, IL 61801, USA
[d] Department of Aerospace Engineering, University of Illinois Urbana-Champaign, Urbana, IL 61801, USA

ARTICLE INFO

Article history:
Received 12 April 2016
Revised 15 August 2016
Accepted 24 September 2016
Available online 8 October 2016

Keywords:
Targeted energy transfer
Cubic nonlinearity
5th order nonlinearity
Vibro-impact
Vehicular drivetrain

ABSTRACT

The automotive industry is predominantly driven by legislations on stringent emissions. This has led to the introduction of downsized engines, incorporating turbocharging to maintain output power. As downsized engines have higher combustion pressures, the resulting torsional oscillations (engine order vibrations) are of broadband nature with an increasing severity, which affect noise and vibration response of the drive train system. Palliative devices, such as clutch pre-dampers and dual mass flywheel have been used to mitigate the effect of transmitted engine torsional oscillations. Nevertheless, the effectiveness of these palliative measures is confined to a narrow band of response frequencies. The nonlinear targeted energy transfer is a promising approach to study vibration mitigation within a broader range of frequencies, using nonlinear vibration absorbers (or nonlinear energy sinks – NESs). These devices would either redistribute vibration energy within the modal space of the primary structure, thus dissipating the vibrational energy more efficiently through structural damping, or passively absorb and locally dissipate a part of this energy (in a nearly irreversible manner) from the primary structure. The absence of a linear resonance frequency of an NES, enables its broadband operation (in contrast to the narrowband operation of current linear tuned mass dampers). Parametric studies are reported to determine the effectiveness of various smooth or non-smooth nonlinear stiffness characteristics of such absorbers. A reduced drivetrain model, incorporating single and multiple absorber attachments is used and comparison of the predictions to numerical integrations proves its efficacy.

* Corresponding author.
E-mail addresses: a.haris@lboro.ac.uk (A. Haris), e.motato@lboro.ac.uk (E. Motato), s.theodossiades@lboro.ac.uk (S. Theodossiades), H.Rahnejat@lboro.ac.uk (H. Rahnejat), pkelly7@ford.com (P. Kelly), avakakis@illinois.edu (A. Vakakis), lbergman@illinois.edu (L.A. Bergman), dmmcf@illinois.edu (D.M. McFarland).

http://dx.doi.org/10.1016/j.apm.2016.09.030
0307-904X/

Nomenclature

NVH	noise vibration and harshness
DMF	dual mass flywheel
CPA	centrifugal pendulum absorber
NES	nonlinear energy sink
TET	targeted energy transfer
NNM	nonlinear normal modes
EO	engine order

1. Introduction

Global exhaust emission legislation requires automotive manufacturers to develop internal combustion engines that produce lower levels of contaminant emissions. The strategy to achieve this goal includes reducing the powertrain weight, downsizing the engine and introducing new technologies, such as hybrid propulsion, cylinder de-activation and start/stop features. Although these technological advances have positive influences in meeting the ever stringent emission legislations, they also introduce broadband, high amplitude torsional oscillations into the lightweight powertrains with potential effects on durability, overall efficiency and poor NVH performance [1–4]. In order to attenuate the torsional oscillations, various palliative measures have been implemented in industry, including Clutch pre-dampers (CD) [5], Dual Mass Flywheel (DMF) [2] and DMF with Centrifugal Pendulum Absorbers (CPAs).

Numerous studies have reported design and working principles of the DMF with CPAs. Bertin et al. [6] performed a comparative study of the performance of radial DMF against a conventional one. Cavina and Serra [7] studied the effect of the DMF on the vehicle NVH characteristics. Theodossiades et al. [8] examined experimentally the effect of the DMF on impact-induced noise in a rear wheel drive light truck. Sun et al. [9] performed a study of nonlinear characteristics of a DMF with radial springs with the objective of optimising key parameters for its improved performance. Other studies include DMFs with magnetorheological damper [10], variable stiffness [11] and arc helix spring [2,12]. Magneto-rheological dampers as visco-lock devices have also been developed and used for NVH refinement in the driveline systems of all wheel drive vehicles [13], where they can act in combined squeeze and shear, attenuating coupled torsional and axial vibrations [14]. The implementation of the DMF has positive effects on vibration reduction, but it increases the inertia of the powertrain system. Furthermore, as it is tuned to a narrow band of frequencies, its effectiveness is limited in downsized, turbocharged engines. With the objective of further enhancing the effectiveness of the DMF a new type of tuned passive absorber, namely, a DMF with CPA [15–17], was used at a cost of increased weight for the potential gains in further suppression of vibration energy during specific drive manoeuvres [18].

Vibration energy of the new generation of internal combustion engines has a broadband spectral content. Therefore, there is a need for effective vibration absorption over a wide range of driving manoeuvres without any prior tuning. The Nonlinear Energy Sink (NES) is a lightweight absorber that can operate over such a broad range of frequencies. It is based on the principle of passive nonlinear targeted energy transfer (TET). TET is a phenomenon, where mechanical (vibration) energy is transferred (in a nearly irreversible manner) from a source (primary structure) to an essentially nonlinear attachment (the NES), where it is partially absorbed, partially redistributed in the frequency domain, and/or dissipated locally [19]. A NES works in two different ways. First, a NES induces energy redistribution within the modal space of the primary structure by scattering the vibrating energy initially concentrated at lower frequency modes into higher frequency ones, where it is dissipated more effectively due to the higher damping capacity of the higher-frequency modes [20]; moreover, the low-to-high frequency vibration energy transfers rapidly reduce the response amplitude of the primary structure. Second, a NES effectively absorbs the undesired vibratory energy through its oscillations with no preferential natural frequency (since it lacks a linear stiffness part) in a nearly irreversible form, providing another way to reduce the vibration amplitudes of the primary structure [21,22].

The literature includes numerous publications dedicated to the understanding of TET and its potential practical applications. Gendelman et al. [23] and Vakakis et al. [24,25] studied NES in two, three and multi-degree-of-freedom (DoF) systems. Vakakis et al. [26] studied the Nonlinear Normal Modes (NNMs) to classify the interaction of NES with the modes of a primary linear system. Jiang et al. [27] studied the effect of NES on the steady-state dynamics of a weakly coupled system. Panagopoulos et al. [28] studied the transient resonant interactions of a finite number of linear oscillators coupled to a NES. Tsakirtzis et al. [29] studied the transient resonant interactions of TET, whilst Kerschen et al. [30] conducted parametric studies to understand the dynamics of energy pumping. McFarland et al. [20] performed investigations in structures with grounded and ungrounded non-linear attachments. Georgiadis et al. [31] studied the shock isolation properties of a linear system coupled to a nonlinear attachment with clearance nonlinearity. Jiang and Vakakis [32] studied the steady state dynamics of systems coupled with smooth and non-smooth strong nonlinearities. Karayannis et al. [33] studied the use of a vibro-impact attachment as a shock absorber. All the above studies have focused on systems with translational DoF, subjected to (mainly) impulsive inputs.

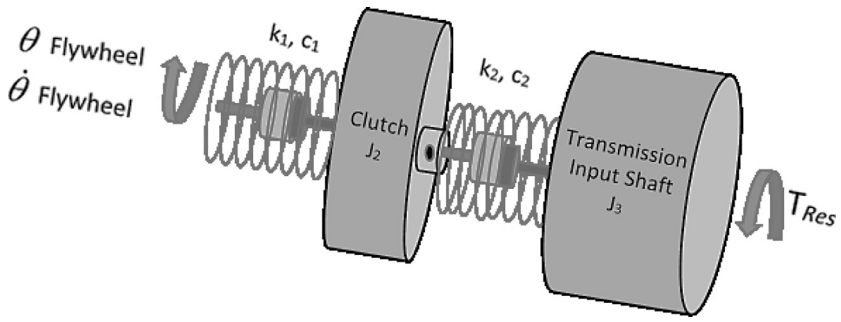

Fig. 1. Schematic representation of the reduced lumped parameter drivetrain model.

There is a dearth of studies in implementing TET in torsional systems. The application of a torsional NES to stabilise a drill-string system was examined in [34]. Gendelman et al. [35] studied numerically and experimentally the dynamics of an eccentric rotational NES mounted inside a linear oscillator. Sigalov et al. [36] expanded the study of Gendelman et al. [35] by analysing the resonance captures and NNMs of the system. Hubbard et al. [37] performed an experimental study on suppressing aeroelastic instabilities of a flexible swept wing using a rotational NES. Through experimental testing it was determined that there is a minimum energy threshold below which TET does not occur. It was also observed that the NES did engage with the first torsional mode of the wing through 1:1 resonance capture.

In vehicular powertrain applications no use of NES is reported to date, yet there are broadband NVH concerns which are of steady state or transient nature and their interplay is of significant concern. They include impulsive broadband action due to impact of transmission gearing, with wave propagation onto thin-walled driveshaft tubes which act as efficient radiators of noise. The phenomenon is commonly referred to as clonk in industry [8,38,39] with a negative effect on customer comfort. On the lower spectral content clutch in-cycle vibration [40] and transmission rattle induced by the repetitive impact of unloaded gear teeth pairs [4,41–44] are both torsional or coupled axial-torsional NVH concerns, which are currently palliated to some extent by the various mass-dampers, slip devices (to dissipate the excess energy) or by the DMF. Therefore, the use of the concepts of TET and NES in dealing with these powertrain concerns is of interest.

A recent study by Haris et al. [45] demonstrated numerically that the NES with purely cubic stiffness can be used efficiently in automotive drivetrains to attenuate torsional vibrations over a broad frequency spectrum; this can be targeted towards attenuation of idle transmission rattle, which is of particular concern with transmitted engine order torsional vibrations to the clutch-transmission system. The frequency range where vibration attenuation was observed correlated to the engine operating between 3300–5500 rpm. However, lower engine speeds are also very important in the general engine operation, particularly for transmission rattle, which is most poignant under engine idling condition (engine speed in the range 600–1000 rpm). The objective of this study is to examine the use of non-smooth and fifth order smooth nonlinear NES stiffnesses on improving the low frequency operation range of the NES. A reduced model of a Front Wheel Drive (FWD) transaxle drivetrain coupled to a three-cylinder turbocharged engine is used in the current analysis. This model is numerically validated using experimental data obtained from vehicle testing. The model is later modified to initially incorporate a third-order NES stiffness, then a vibro-impact NES and finally a NES with fifth-order NES stiffness. Then, the effect that a NES with smooth and non-smooth nonlinear stiffness have on the attenuation of torsional oscillations at low frequency ranges is analysed. Finally, the main conclusions of this study and suggestions for future work are provided.

2. Drivetrain model validation

The drivetrain of a forward drive transaxle powertrain equipped with a three cylinder engine is modelled. The system uses a Solid Mass Flywheel (SMF) and a clutch pre-damper. Modelling the entire drivetrain system can be computationally intensive, thus a simplified 2- DOF torsional lumped parameter model (Fig. 1) is used to examine the proposed TET concept.

The reduced model includes the inertia of the clutch assembly (J_2) and the transmission input shaft inertia (J_3). The engine-flywheel assembly is excluded from the numerical model, but the measured motion of the flywheel, including engine order harmonics is used as an input to the clutch assembly, denoted by $\theta_{Flywheel}$ and $\dot{\theta}_{Flywheel}$. As the model excludes the other drivetrain components, their effect on the transmission input shaft is represented by the resisting torque T_{RES}. Using first principles, the linear dynamic model of the system yields:

$$\begin{bmatrix} J_2 & 0 \\ 0 & J_3 \end{bmatrix} \begin{bmatrix} \ddot{\theta}_2 \\ \ddot{\theta}_3 \end{bmatrix} + \begin{bmatrix} c_2 + c_1 & -c_2 \\ -c_2 & c_2 \end{bmatrix} \begin{bmatrix} \dot{\theta}_2 \\ \dot{\theta}_3 \end{bmatrix} + \begin{bmatrix} k_2 + k_1 & -k_2 \\ -k_2 & k_2 \end{bmatrix} \begin{bmatrix} \theta_2 \\ \theta_3 \end{bmatrix} = \begin{bmatrix} k_1\theta_{Flywheel} + c_1\dot{\theta}_{Flywheel} \\ -T_{Res} \end{bmatrix} \tag{1}$$

where, θ_2 and θ_3 are the angular displacements of the clutch and the transmission input shaft, respectively. $k_1\theta_{Flywheel} + c_1\dot{\theta}_{Flywheel}$ is the input torque applied to the clutch assembly, which is a function of the flywheel motion. Typical range of parameter values for torsional linear stiffness k_1, k_2 and inertial components J_2 and J_3 are listed in Table 1.

Table 1
Typical model parameters.

Inertia [kgm^2]	Stiffness [Nm/rad]
$J_2 = 0.001–0.01$	$k_1 = 1000–1500$
$J_3 = 0.003–0.015$	$k_2 = 15{,}000–25{,}000$

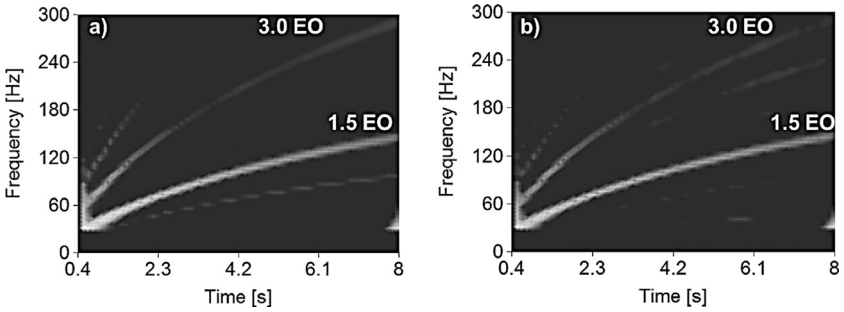

Fig. 2. (a) CWT of numerical predictions and (b) CWT of the experimental measurements for the manoeuvre in 1st gear at 25% throttle.

The resisting torque T_{Res} is modelled as a function of the aerodynamic drag torque T_{AERO} and the tyre rolling resisting torque, T_R

$$T_{AERO} = \frac{1}{2}\rho S C_d V^2 r_w \tag{2}$$

$$T_R = \left[P^{\alpha} N^{\beta}\left(A + B v_{hub} + C v_{hub}^2\right)\right] r_w \tag{3}$$

Thus:

$$T_{Res} = T_{AERO} + T_R \tag{4}$$

where, P is the tyre pressure; N is the tyre normal load; α, β, A, B *and* C are coefficients; v_{hub} is the wheel hub velocity; r_w is the laden tyre radius; ρ is the density of air; S is the vehicle frontal area; C_d is the aerodynamic coefficient of drag and V is the vehicle longitudinal velocity.

The coefficients c_1 and c_2 of the damping matrix **[C]** were obtained using Caughey's method as

$$[C] = \begin{bmatrix} J_2 & 0 \\ 0 & J_3 \end{bmatrix} \mathbf{\Phi}[\boldsymbol{Z}]\mathbf{\Phi}^T \begin{bmatrix} J_2 & 0 \\ 0 & J_3 \end{bmatrix}, \tag{5}$$

where $\mathbf{\Phi}$ is the modal matrix obtained through the generalised eigenvalue problem and $[\boldsymbol{Z}]$ is the diagonal matrix of the modal damping:

$$[\boldsymbol{Z}] = \begin{bmatrix} 2\zeta_1\omega_1 & 0 \\ 0 & 2\zeta_2\omega_2 \end{bmatrix}, \tag{6}$$

where ζ_i is the damping ratio of the ith mode, corresponding to the natural frequency ω_i. Damping ratios $\zeta_1 = 0.8$ and $\zeta_2 = 0.5$ corresponding to the natural frequencies $\omega_1 = 60$ Hz and $\omega_2 = 800$ Hz (approximate values) were selected to obtain good conformance between the model and experimental results in both time and frequency domains.

Using Eqs. (1)–(6), a Matlab/Simulink code is developed to simulate the drivetrain response. The model results are compared with the experimental measurements obtained from a vehicle equipped with a similar powertrain. The experimental measurements are obtained through use of sensors mounted onto the flywheel and the transmission input shaft. An appropriate variable sampling rate was employed. The manoeuvre introduced in the numerical model simulates engine operation when engaged in 1st gear with 25% fixed throttle over the entire engine speed range. The duration of the test is 8 s.

The numerical model is validated both in frequency and time domains. For the frequency domain, the Continuous Wavelet Transform (CWT) method is used to obtain the transient spectral content at the various Engine Order (EO) harmonics (these are the multiples of the crankshaft's rotational speed [5]). The CWT plot in Fig. 2 is obtained using AutoSignal software. It shows the presence of the various EO harmonics. For the 3-cylinder 4-stroke engine investigated here, the 1.5 EO harmonic is the most significant contribution to the oscillatory response [5]. This is because combustion occurs thrice over two crankshaft revolutions. It can be observed from the plot in Fig. 2 that the frequency content of both the experimental and numerical responses exhibit similar behaviour. The time domain response in Fig. 3 compares the numerically obtained angular velocity of the transmission input shaft with that acquired experimentally. It can be observed that very good correlation exists between the numerical predictions and measurements. In addition, the insets to the same figure show the CWT plots at two different speeds, highlighting again good correlation in the frequency domain. For further validation of

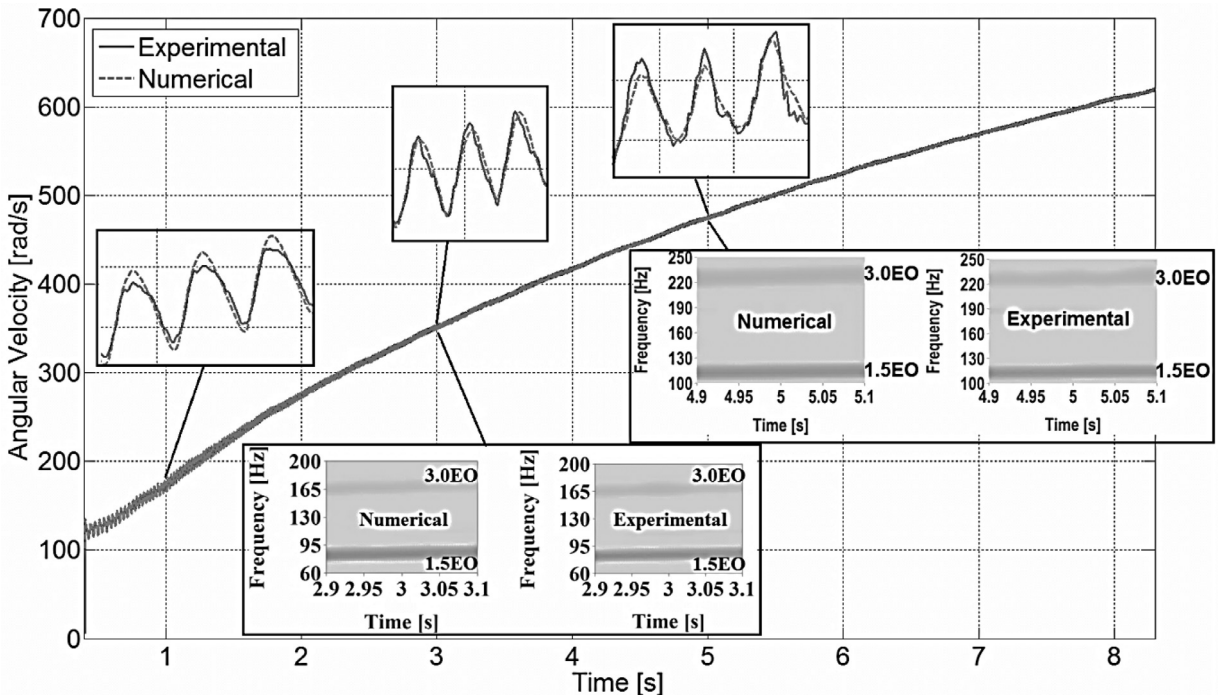

Fig. 3. Numerical and experimental time histories of the transmission input shaft velocity with local CWT insets for the manoeuvre in 1st gear at 25% throttle.

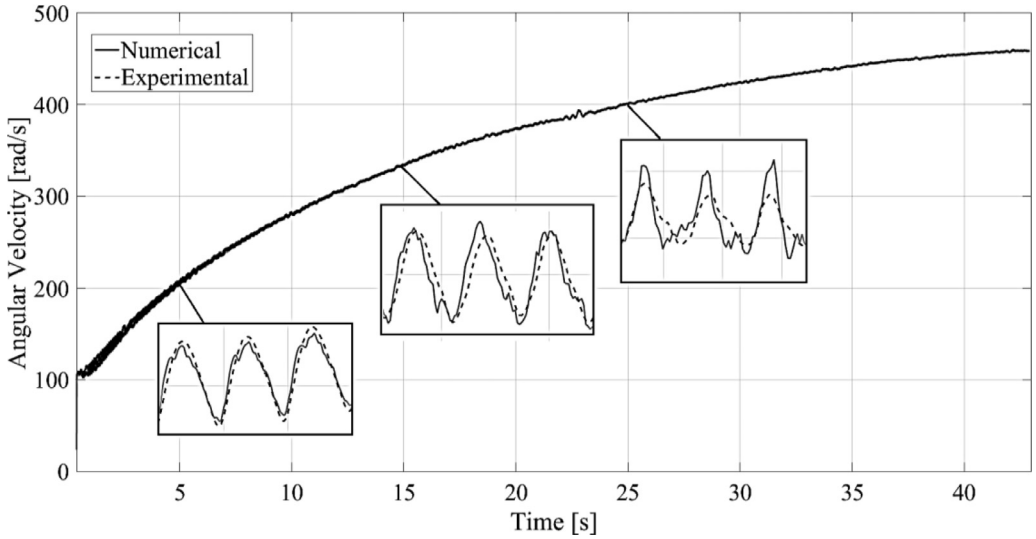

Fig. 4. Numerical and experimental time histories of the transmission input shaft velocity for the manoeuvre in 2nd gear at 25% throttle.

the numerical model, the process was repeated for different manoeuvres as well and as an example for the time domain response of the 2nd Gear engaged at 25% fixed throttle. This is shown in Fig. 4.

3. Drivetrain model coupled with an NES attachment

The 2-DOF torsional lumped drivetrain model is modified to incorporate a single cubic NES attachment (Fig. 5). The NES is coupled in parallel with the clutch friction disc through an essentially nonlinear torsional cubic spring of constant stiffness k_N and a linear viscous damper with damping coefficient of c_N. The differential equations of motion describing the dynamics of the powertrain with the integrated NES are given in (7). The manoeuvre, simulating the transmission in 1st gear with 25% throttle is used to assess the performance of the NES

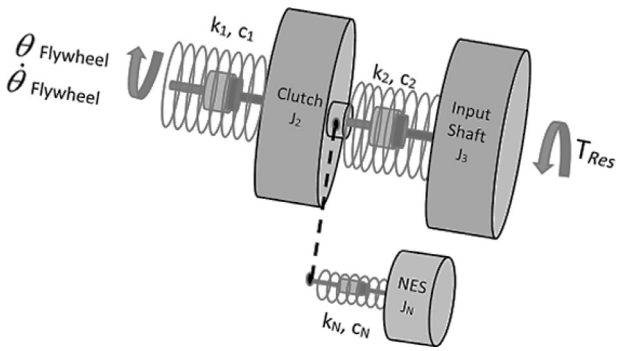

Fig. 5. Linear powertrain model equipped with a single cubic NES attachment.

$$\begin{bmatrix} J_2 & 0 & 0 \\ 0 & J_3 & 0 \\ 0 & 0 & J_N \end{bmatrix} \begin{bmatrix} \ddot{\theta}_2 \\ \ddot{\theta}_3 \\ \ddot{\theta}_N \end{bmatrix} + \begin{bmatrix} c_1 + c_2 + c_N & -c_2 & -c_N \\ -c_2 & c_2 & 0 \\ -c_N & 0 & c_N \end{bmatrix} \begin{bmatrix} \dot{\theta}_2 \\ \dot{\theta}_3 \\ \dot{\theta}_N \end{bmatrix} + \begin{bmatrix} k_2 + k_1 & -k_2 & 0 \\ k_2 & k_2 & 0 \\ 0 & 0 & 0 \end{bmatrix} \begin{bmatrix} \theta_2 \\ \theta_3 \\ \theta_N \end{bmatrix}$$
$$= \begin{bmatrix} k_1\theta_{Flywheel} + c_1\dot{\theta}_{Flywheel} - k_N(\theta_2 - \theta_N)^3 \\ -T_{Res} \\ k_N(\theta_2 - \theta_N)^3 \end{bmatrix}. \tag{7}$$

To assess the effectiveness of the NES attachment, the performance of the system with *locked* NES (i.e., with the nonlinear stiffness of the NES locked so that the NES contributes to the dynamics only through its inertia) is compared with that of a system with an *active* NES (with the nonlinear NES stiffness and viscous damper enabled to operate). The matrix formulation for the *locked* system is

$$\begin{bmatrix} J_2 + J_N & 0 \\ 0 & J_3 \end{bmatrix} \begin{bmatrix} \ddot{\theta}_2 \\ \ddot{\theta}_3 \end{bmatrix} + \begin{bmatrix} c_2 + c_1 & -c_2 \\ -c_2 & c_2 \end{bmatrix} \begin{bmatrix} \dot{\theta}_2 \\ \dot{\theta}_3 \end{bmatrix} + \begin{bmatrix} k_2 + k_1 & -k_2 \\ -k_2 & k_2 \end{bmatrix} \begin{bmatrix} \theta_2 \\ \theta_3 \end{bmatrix} = \begin{bmatrix} k_1\theta_{Flywheel} + c_1\dot{\theta}_{Flywheel} \\ -T_{Res} \end{bmatrix}. \tag{8}$$

A criterion that compares the severity of the 1.5 engine order (EO) harmonic response of the transmission input shaft acceleration in the *locked* and *active* systems is used as a performance measure. The logic behind selecting this specific EO as the performance measure is that it is the fundamental firing order of the considered engine combustion signature. Therefore, the generated torsional vibrations are expected to possess the highest energy content at this frequency. By analysing the performance of the NES at this specific EO it is possible to identify the frequency range, where the NES provides some degree of vibration attenuation. It is important to note that the identification of the frequency range is simply a method for verifying the performance of the NES. This does not imply that the NES is a frequency-dependent absorber. An NES that is tuned to suppress the vibrations in a specific range of frequencies would still function in all scenarios provided that the applied input energy is within its operating threshold.

The Matlab command *Pwelch* is used to obtain the resultant acceleration amplitudes of both *active* and *locked* systems. This computes the Power Spectral Density (PSD) of the transmission input shaft acceleration using Welch's overlapped segment averaging estimator. The resultant PSD has the unit of $\frac{(input\ signal)^2}{frequency}$. In order to compute the PSD, the acceleration signals are provided as inputs to the command, which returns the corresponding PSD with the unit of $rad^2/s^4/Hz$. Therefore, to obtain the 1.5 EO acceleration, the product of PSD × Frequency is square rooted, i.e. $1.5\ EO = \sqrt{PSD \times Frequency}$, where frequency is the 1.5 EO harmonic.

Schaeffler [46] reported that using centrifugal pendulum-type absorbers for three-cylinder engines, acceptable acceleration values of 500 rad/s² for engine speed of 1000 rpm are attainable. It is argued that the acceleration amplitudes can still be significantly reduced if the entire clutch system – DMF with centrifugal pendulum-type absorber and clutch – is designed according to an entirely new layout. Then, it is possible to achieve angular acceleration amplitudes below 200 rad/s² from engine speeds of 800 rpm upwards [46]. Clearly, further reduction of the torsional oscillations would be quite beneficial. The successful incorporation of TET could potentially be a step towards achieving lower levels of acceleration amplitudes at the transmission input shaft. Such an outcome would be desirable for attenuation of transmission rattle.

A series of simulations were performed for the range of nonlinear stiffness $k_N = 10^4$ - $10^7 = Nm/rad^3$ and inertia of $J_N = 8 - 15\ \%$ of the transmission input shaft with a damping coefficient of $c_N = 0.001\ Nms/rad$. The powertrain model with the cubic NES attachment is used for the engine operating in 1st gear with 25% throttle over the entire engine speed sweep. The result of the numerical simulation is presented in the form of a contour plot. The plot highlights the Area of Effective Acceleration Amplitude Reduction (AEAAR), which is calculated through integration using the trapezoidal rule in Eq. (9). This method evaluates the area under the acceleration amplitude curve (Fig. 6) for both the *locked* and *active* NES. The difference between the resultant areas is the AEAAR, shown in Fig. 6.

$$AEAAR = Trapz\ (Acc_L, Freq_L)\ -\ Trapz\ (Acc_A, Freq_A) \tag{9}$$

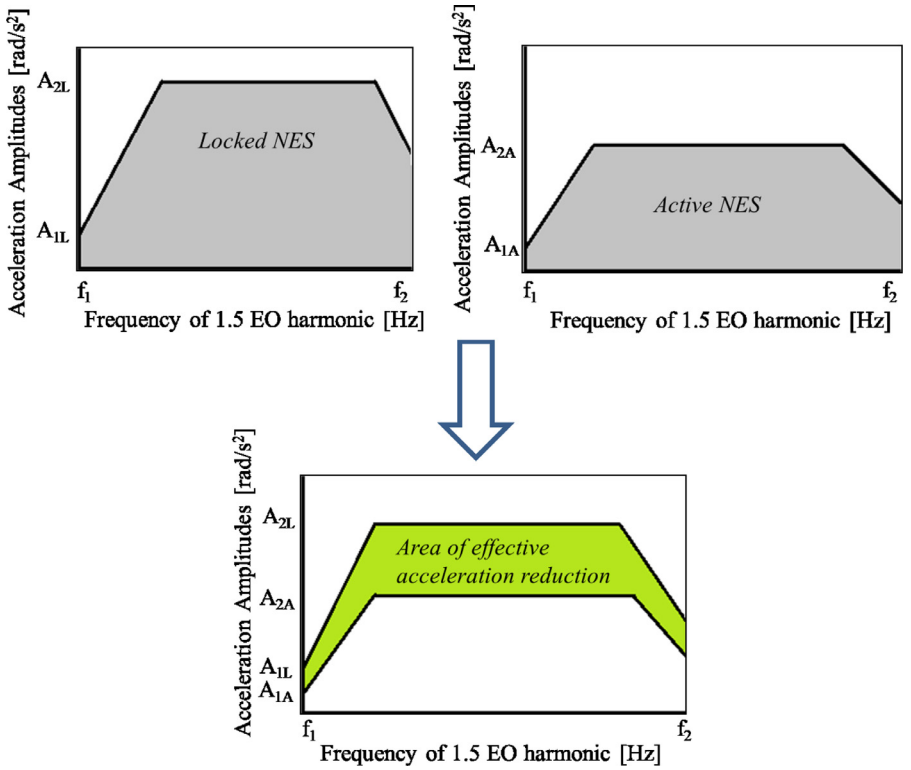

Fig. 6. Quantification of the Area of Effective Acceleration Amplitude Reduction (AEAAR).

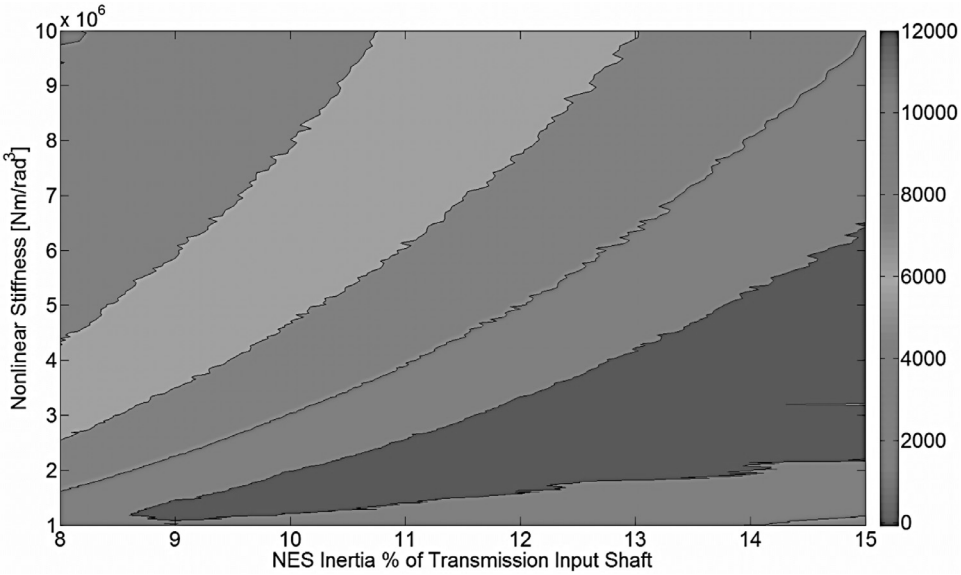

Fig. 7. Contour plot identifying the area of effective acceleration reduction for a drivetrain equipped with a single cubic NES with engine operating in 1st gear and with 25% fixed throttle.

where,

$$Freq_L = 1.5\ EO\ frequency\ of\ the\ \ locked\ system$$
$$Acc_L = Acceleration\ \ amplitudes\ \ of\ \ the\ \ locked\ \ system$$
$$Freq_A = 1.5\ EO\ \ frequency\ of\ \ the\ active\ system$$
$$Acc_A = Acceleration\ \ amplitudes\ \ of\ \ the\ active\ system$$

Using the pre-defined ranges of nonlinear stiffness coefficient and the NES inertia, a contour plot is shown in Fig. 7. The abscissa of the plot shows the variation of NES inertia as a percentage of the transmission input shaft inertia. The ordinate

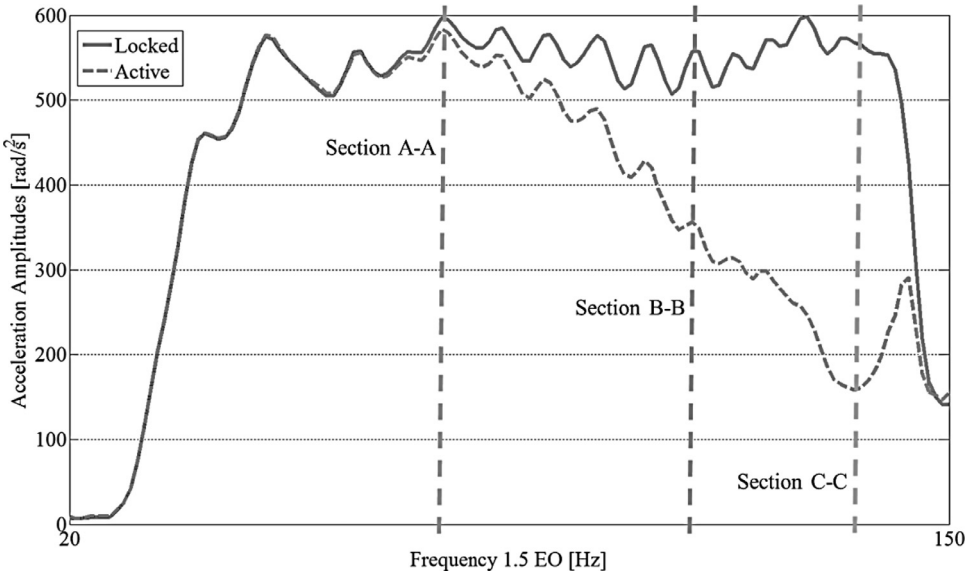

Fig. 8. Acceleration amplitudes of the 1.5 EO at the transmission input shaft with NES parameters ($J_N = 11\%$ of transmission input shaft inertia, $k_N = 2 \times 10^6$ Nm/rad^3 and $c_N = 0.001$ Nms/rad).

of the plot shows the variation of the cubic nonlinear stiffness. The shaded regions represent the AEAAR. The contour plot in Fig. 7. indicates that for stiffness values above 6×10^{-6} Nm/rad^3 and NES inertias below 10% of the transmission input shaft inertia, the AEAAR is less than 5000 rad-Hz/s^2. This implies that the NES would not induce any significant attenuation on the transmission input shaft oscillatory acceleration. Conversely, when any of the NES parameters demarcated by the darker area on the contour plot are selected, the NES performance is improved and maximum vibration attenuation is achieved (AEAAR = 12,000 rad-Hz/s^2). For this particular analysis, the NES parameters are selected as $J_N = 11\%$ of the transmission input shaft inertia, $k_N = 2 \times 10^6$ Nm/rad^3, and $c_N = 0.001$ Nms/rad. The selection of NES inertia should consider the overall driveline weight which is an essential design criterion for modern powertrain systems.

The corresponding 1.5 EO acceleration contribution of the transmission input shaft for the selected parameters is shown in Fig. 8. Significant vibration attenuation is achieved over a broad spectrum of frequencies with the minimum acceleration amplitude obtained at 180 rad/s^2

The time domain behaviour of the transmission input shaft angular velocity (*locked* and *active*) is shown in Fig. 9. It is observed that at around 3 s, the amplitude of oscillations of the active NES system is slightly attenuated (550 rad/s^2), corresponding to section A-A in Fig. 8. Furthermore, around 5 s, there is a clear amplitude reduction for the NES *active* system when compared with its *locked* state. This corresponds to the section B-B in Fig. 8. Around 7 s, the amplitude of oscillations for the *active* NES system is at minimum (section C-C in Fig. 8). From the predictions, it can be concluded that for this particular set of NES parameters and input excitation, a single cubic NES is able to efficiently attenuate the vibration frequencies in the upper half of the frequency response plot

A similar numerical analysis was performed in order to target low frequency ranges with a cubic NES. The NES parameters obtained for this case were: $J_N = 7\%$ of the transmission input shaft inertia and $k_N = 0.2 \times 10^4$ Nm/rad^3. The NES damping coefficient is similar to the previous analysis at $c_N = 0.001$ Nms/rad. Fig. 10 shows that there is significant attenuation in the frequency range 50–70 Hz. The question at this point is whether it is possible to extend this frequency range through the use of different classes of nonlinear stiffness. This is the study presented in the next section

4. Drivetrain system coupled with smooth / non-smooth NES attachment

Simulations have demonstrated that although vibration attenuation is achieved in both the high and low frequency ranges, this is not achieved in a broadband manner. The objective now is to study the effect that two different nonlinear stiffnesses have on vibration suppression. Referring back to Fig. 10, broadband attenuation with a cubic NES is not observed. Furthermore, the results presented in [25,31,33] concluded that broadband vibration suppression could only be achieved through the use of vibro-impact (VI) NES or higher orders of smooth nonlinearity.

The first class of NES analysed is a vibro-impact (VI NES), as shown in Fig. 11. The second class is an NES with a fifth order smooth nonlinear stiffness coefficient. The study is based on an extensive series of simulations to compare the acceleration amplitude of the 1.5 E.O harmonic of the gearbox input shaft when the NES absorber is either *active* or remains *locked*. In total 130,000 parameter combinations were examined for a typical vehicle manoeuvre with an 8 s duration, corresponding to the accelerative motion of the vehicle in 1st gear at 25% open throttle. During this manoeuvre the speed of

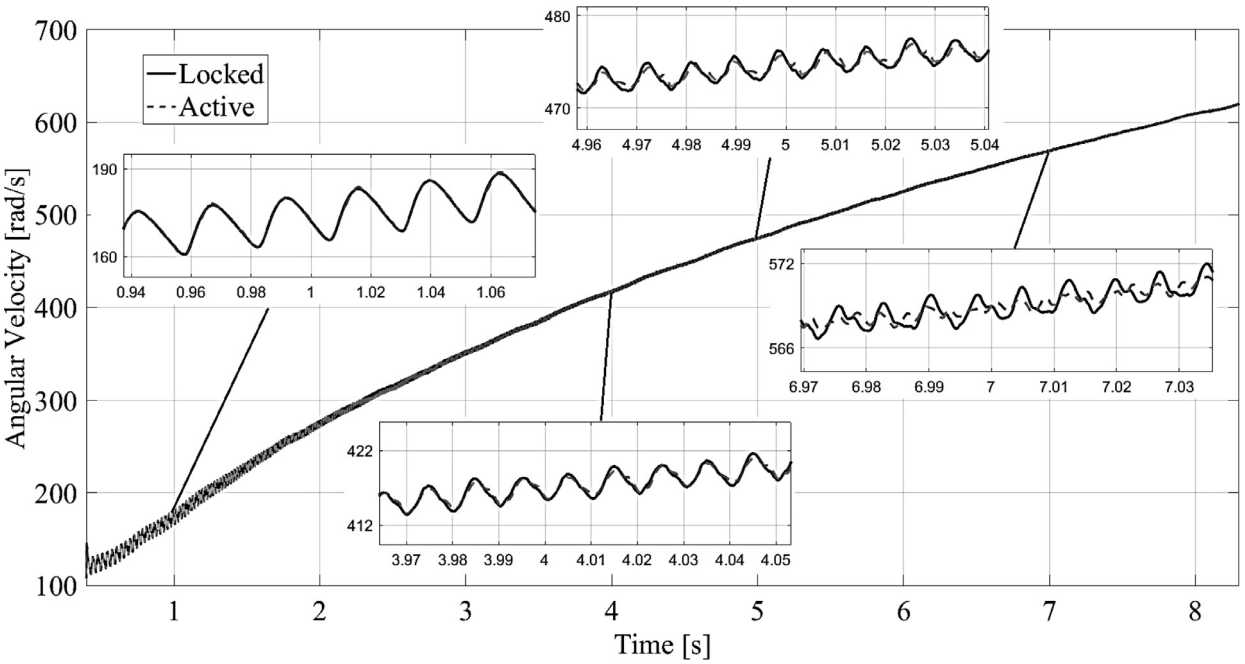

Fig. 9. Comparison of the time history of angular velocity of the transmission input shaft for the locked and active cubic NES systems.

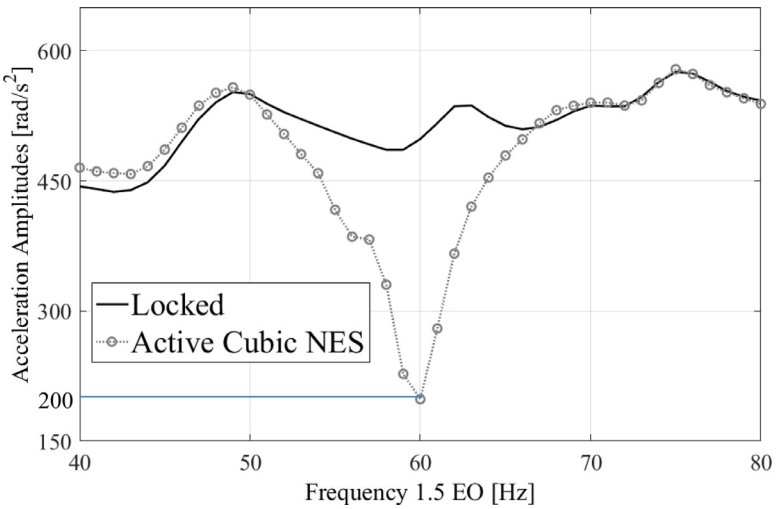

Fig. 10. Acceleration amplitude of the transmission input shaft for a drivetrain equipped with a single cubic NES targeting lower frequencies.

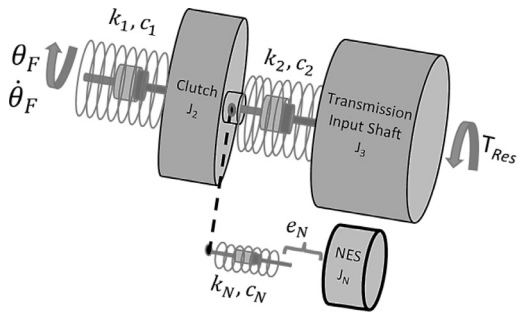

Fig. 11. Schematic representation of the drivetrain model equipped with a single vibro-impact NES.

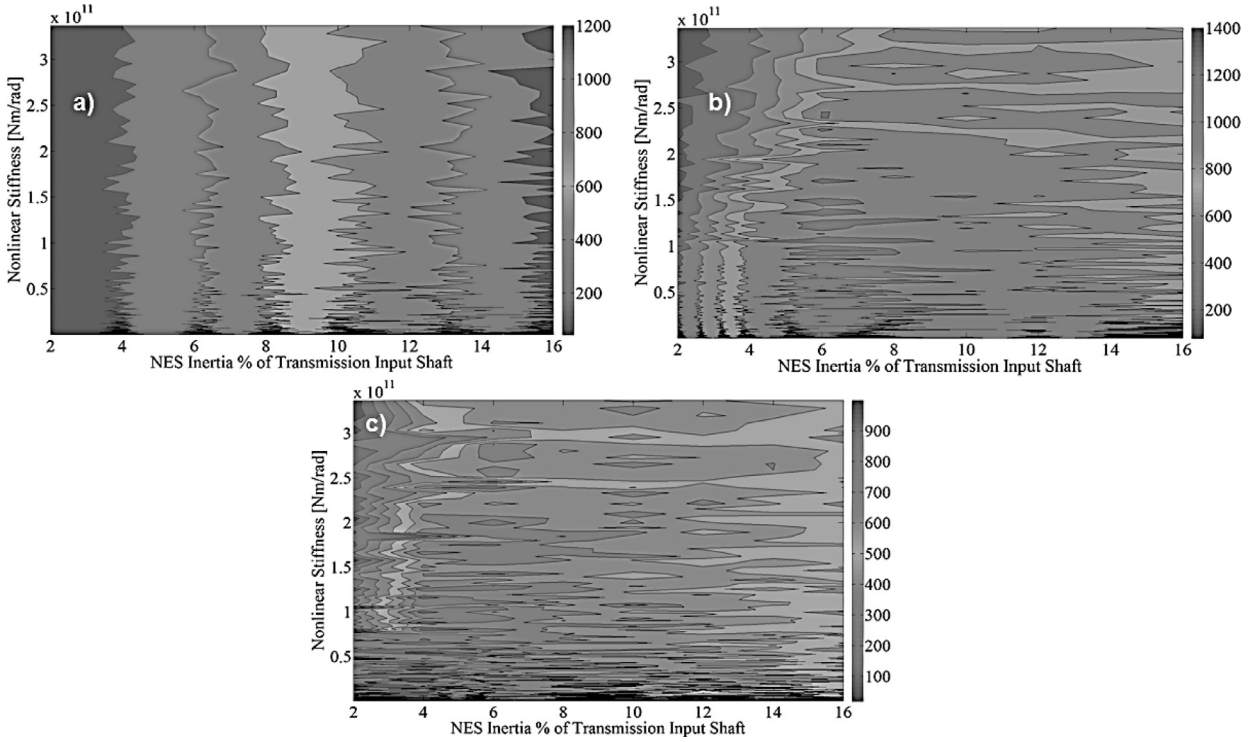

Fig. 12. Area of Effective Acceleration Reduction for 1.5 EO response resident on the transmission input shaft with c_N= 0.001 Nms/rad and clearance (a) 0.006 rad (b) 0.036 rad, and (c) 0.066 rad.

the engine increases from 990 to 5900 rpm. The AEAAR is calculated for multiple combinations of NES stiffness and inertia. For all the studied cases the damping coefficient c_N is assumed to be 0.001 Nms/rad.

4.1. Single vibro-impact NES

A single VI attachment with inertia J_N, stiffness k_N, damping c_N and clearance e_N is coupled to the clutch disc. The equations of motion in matrix form become

$$\begin{bmatrix} J_2 & 0 & 0 \\ 0 & J_3 & 0 \\ 0 & 0 & J_n \end{bmatrix}\begin{bmatrix} \ddot{\theta}_2 \\ \ddot{\theta}_3 \\ \ddot{\theta}_n \end{bmatrix} + \begin{bmatrix} k_1+k_2 & -k_2 & 0 \\ -k_2 & k_2 & 0 \\ 0 & 0 & 0 \end{bmatrix}\begin{bmatrix} \theta_2 \\ \theta_3 \\ \theta_n \end{bmatrix} + \begin{bmatrix} c_1+c_2 & -c_2 & 0 \\ -c_2 & c_2 & 0 \\ 0 & 0 & 0 \end{bmatrix}\begin{bmatrix} \dot{\theta}_2 \\ \dot{\theta}_3 \\ \dot{\theta}_n \end{bmatrix} + \begin{bmatrix} F_{kn} \\ 0 \\ -F_{kn} \end{bmatrix} = \begin{bmatrix} k_1\theta_F + c_1\dot{\theta}_F \\ -T_{RES} \\ 0 \end{bmatrix} \tag{10}$$

where:

$$F_{kn} = \begin{cases} k_n(\theta_2 - \theta_n - e_n) + c_n\left(\dot{\theta}_2 - \dot{\theta}_n\right) & \theta_2 - \theta_n \geq e_n \\ 0 & -e_n < \theta_2 - \theta_n < e_n \\ k_n(\theta_2 - \theta_n + e_n) + c_n\left(\dot{\theta}_2 - \dot{\theta}_n\right) & \theta_2 - \theta_n \leq -e_n \end{cases}$$

Simulations are reported for a range of NES inertias (J_N=*2–16 % of the transmission input shaft inertia*) and NES stiffness ($k_N = 10^7$ - 10^{11} *Nm/rad*). The damping is kept constant and equal to the damping used for the previously described cubic NES (i.e. c_N= *0.001 Nms/rad*). The high linear stiffness range is chosen to allow the NES to reach the vibro-impact limit, which is generally achieved when $k_N \to \infty$. Three different clearance values e_n of 0.006 rad, 0.036 rad and 0.066 rad are used and in each case the AEAAR is calculated. The choice of clearance is based on two factors. First, the amplitude of oscillations of the NES should be large enough to overcome the clearance limit and to be able to interact with the spring k_N [31]. Second, the clearance should allow for quick dissipation of the impact energy. Higher clearance values are not a feasible option as no vibro-impacts can occur [33]. Simulations show that this range of stiffness and clearance activates the NES at the required low frequency range. It is noteworthy that the attenuation of low frequencies is of particular interest in the palliation of the

Table 2
Vibro-Impact NES parameters resulting in maximum AEAAR.

Clearance (radians)	NES inertia as a % of transmission input shaft inertia	NES Stiffness (Nm/rad)	Maximum AEAAR (rad-Hz/s^2)
$e_N = 0.006$	$J_N = 16$	10^{11}	1200
$e_N = 0.036$	$J_N = 6$	10^{11}	1400
$e_N = 0.066$	$J_N = 6$	$2x10^{11}$	900

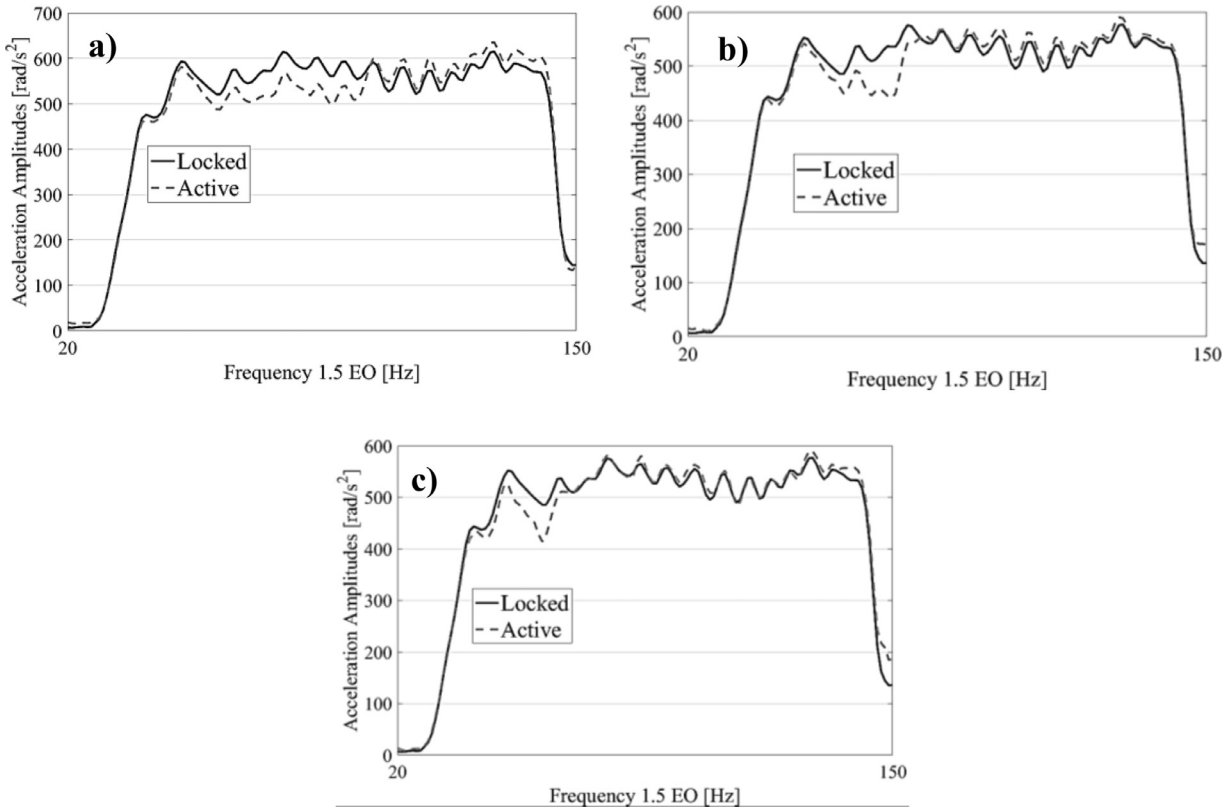

Fig. 13. Contribution of 1.5 EO harmonic acceleration amplitude of the transmission input shaft for three different optimal cases in Table 2 for clearances of (a) 0.006 rad (b) 0.036 rad, and (c) 0.066 rad.

transmission rattle [4,41–44].The AEAAR results are summarized in the three contour plots of Fig. 12 and the optimal cases (where the AEAAR becomes maximum) are listed in Table 2.

The NES parameters of the three optimal clearance cases in Table 2 are used to plot the corresponding transmission input shaft acceleration amplitudes at the 1.5 E.O harmonic for the locked and active systems (Fig. 13). The results show that low frequencies can be targeted for the NES with clearance of $e_N = 0.006\,rad$ (Fig. 13a). As the specific energy level entered in the system for this particular case (typical vehicle manoeuvre with 1st gear engaged at 25% open throttle) is not sufficient to activate the TET mechanism, significant vibration attenuation is not achieved and high acceleration amplitudes remain. For the first clearance case, the noted negligible improvement is further confirmed in the time domain (Fig. 14), where no substantial vibration attenuation of the transmission input shaft's angular velocity is observed. For the other two clearance cases, there has been a reduction in the acceleration amplitudes (Fig. 13b and c). The improvement is noted for a narrow band of frequencies. The ineffectiveness of the VI NES for this specific application may be explained as follows. First, a relatively high spring stiffness is used in the numerical analysis. This restricts the motion of the NES and results in only a small relative displacement between the clutch and the NES. Second, the applied input energy may be insufficient to activate TET and as a consequence significant vibration attenuation is not achieved. NES with lower stiffness values is also investigated. This essentially results in the NES performing as a piecewise linear system, exhibiting a similar performance to a cubic NES, tuned to target higher frequency vibrations only.

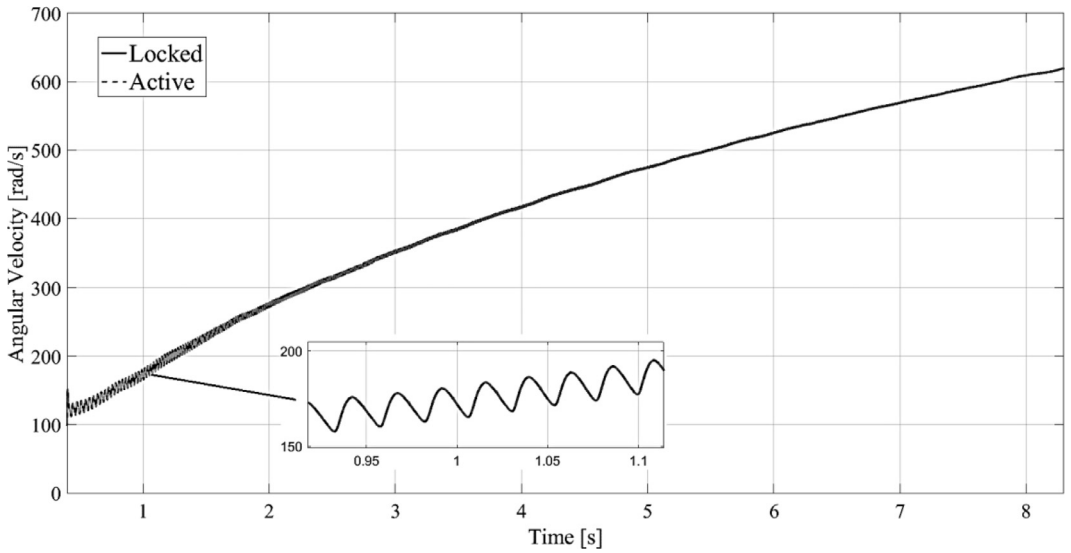

Fig. 14. Transmission input shaft angular velocity for NES with clearance $e_N = 0.006$ rad, $J_N = 16\%$ of the transmission input shaft inertia, $k_N = 10^{11}$ Nm/rad and $c_N = 0.001$ Nms/rad.

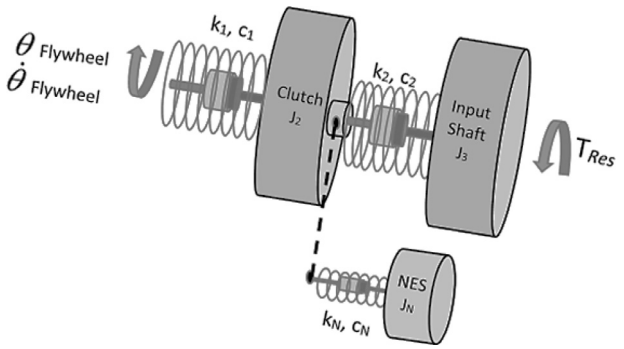

Fig. 15. Schematic representation of the drivetrain equipped with a single 5th order NES.

4.2. Linear powertrain model with 5th Order NES stiffness

A single fifth order NES (Fig. 15) with inertia J_N and stiffness k_N is coupled to the clutch disc. The NES damping coefficient is kept constant as in the previous analysis, $c_N = 0.001$ Nms/rad. The equations of motion in matrix form become:

$$\begin{bmatrix} J_2 & 0 & 0 \\ 0 & J_3 & 0 \\ 0 & 0 & J_N \end{bmatrix} \begin{bmatrix} \ddot{\theta}_2 \\ \ddot{\theta}_3 \\ \ddot{\theta}_n \end{bmatrix} + \begin{bmatrix} k_1 + k_2 & -k_2 & 0 \\ -k_2 & k_2 & 0 \\ 0 & 0 & 0 \end{bmatrix} \begin{bmatrix} \theta_2 \\ \theta_3 \\ \theta_N \end{bmatrix} + \begin{bmatrix} c_1 + c_2 & -c_2 & 0 \\ -c_2 & c_2 & 0 \\ 0 & 0 & 0 \end{bmatrix} \begin{bmatrix} \dot{\theta}_2 \\ \dot{\theta}_3 \\ \dot{\theta}_N \end{bmatrix} = \begin{bmatrix} k_1\theta_F + c_1\dot{\theta}_F - k_N(\theta_2 - \theta_N)^5 \\ -T_{Res} \\ k_N(\theta_2 - \theta_N)^5 \end{bmatrix} \tag{11}$$

The parameters of the fifth order NES are tuned to target low response frequencies. The NES inertia is varied in the range: $J_N = 2 - 10\%$ of the transmission input shaft inertia. The NES stiffness is varied in the range: $k_N = 10^3 - 4 \times 10^4$ Nm/rad^5. The model is excited with the same typical vehicle manoeuvre used in the vibro-impact case (1st gear engaged at 25% throttle). The AEAAR is calculated for multiple combinations of stiffness and inertia to generate the contour plot of Fig. 16. The optimal case (where AEAAR attains its maximum value) is achieved when $J_N = 6\%$ of the transmission input shaft inertia, $k_N = 4 \times 10^4$ Nm/rad^5 and the corresponding AEAAR is 2500 (rad-Hz/s^2). This AEAAR value is almost twice the maximum value achieved with the VI NES.

The 1.5 EO harmonic acceleration contributions of the transmission input shaft for the optimal case of fifth order NES are plotted in Fig. 17. To compare the effectiveness of the fifth order NES with the performance of an optimized cubic NES, tuned to low frequencies, the gearbox input shaft acceleration of both systems are plotted in the same frequency range and compared with the locked system. These two classes of NES absorbers have similar behaviour and no substantial benefit is achieved by using the higher order nonlinearity. In addition, the results show that 5th order NES requires slightly increased

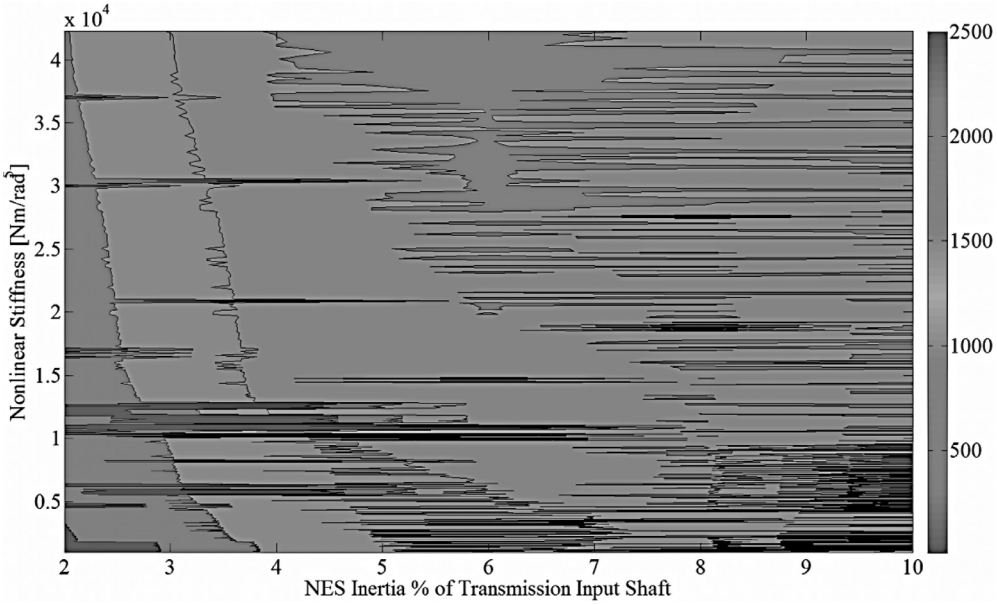

Fig. 16. Area of Effective Acceleration Reduction of 1.5 E.O transmission input shaft for NES with fifth order nonlinear stiffness coefficient.

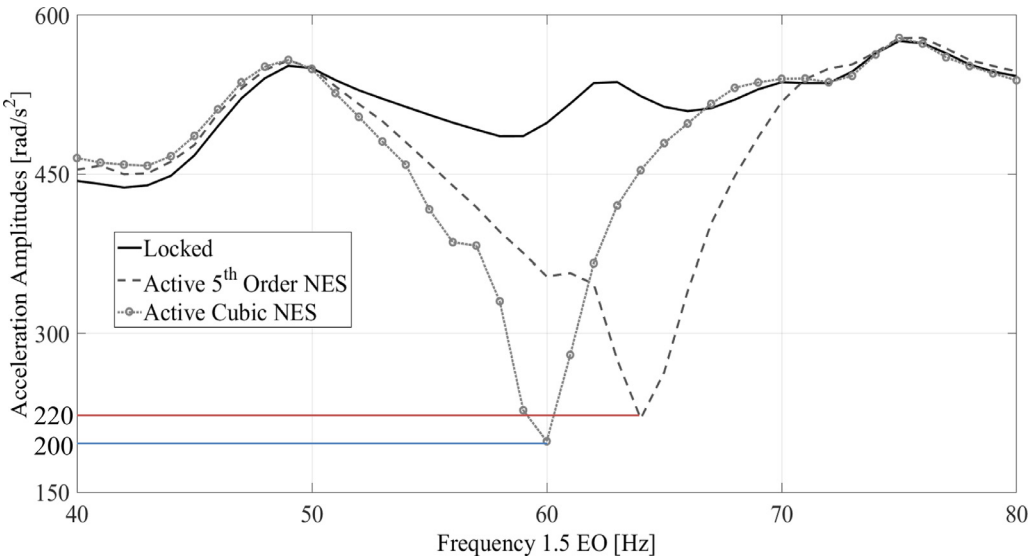

Fig. 17. Spectra of the 1.5 EO harmonic acceleration amplitude of the transmission input shaft for drivetrains equipped with fifth order and cubic NESs.

inertia and higher nonlinear stiffness in order to attenuate vibrations in the same range of frequencies as the cubic NES. It is not practically feasible to use a 5th order NES when a cubic NES would suffice, because it is more difficult to produce the physical springs with fifth order nonlinearity. Conversely, cubic nonlinearity is more easily realizable using metallic wire, for example.

4.3. Linear drivetrain model with vibro-impact NES and cubic NES

Finally, a pair of parallel NES (Fig. 18) is considered in order to determine if their interactions can induce the required vibration attenuation at low frequencies. The first NES is a cubic attachment, tuned to target high frequencies. The second NES is a vibro-impact attachment tuned to target low frequencies. Both attachments are coupled in parallel to the clutch

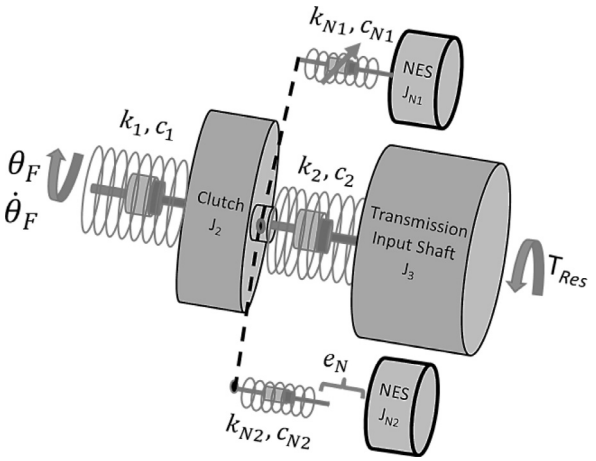

Fig. 18. Drivetrain model coupled in parallel to a Vibro-Impact NES and a Cubic NES.

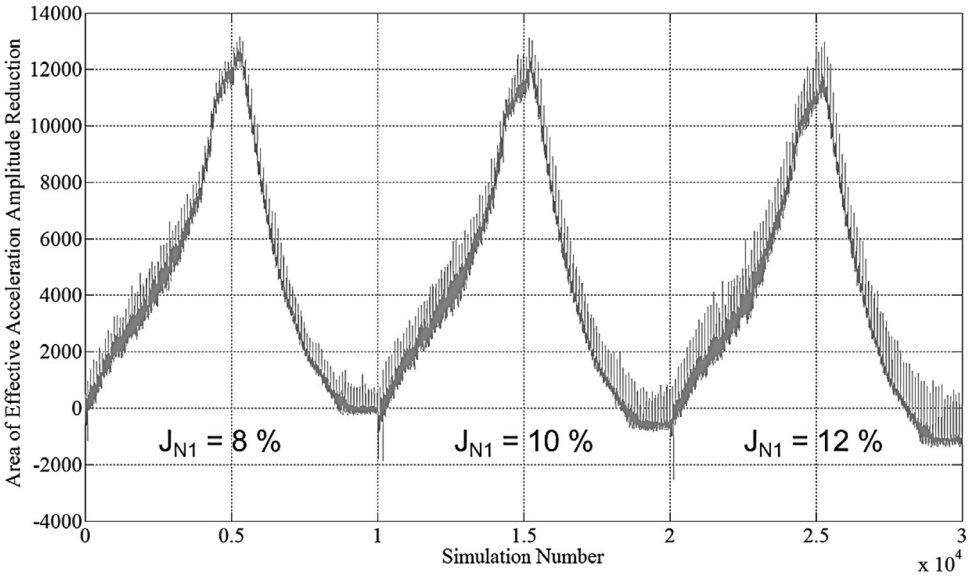

Fig. 19. Area of Effective Acceleration Amplitude Reduction for two parallel NES for different cubic NES inertias.

disc. The equations of motion for this system in matrix form are

$$\begin{bmatrix} J_2 & 0 & 0 & 0 \\ 0 & J_3 & 0 & 0 \\ 0 & 0 & J_{N1} & 0 \\ 0 & 0 & 0 & J_{N2} \end{bmatrix} \begin{bmatrix} \ddot{\theta}_2 \\ \ddot{\theta}_3 \\ \ddot{\theta}_N \\ \ddot{\theta}_{N2} \end{bmatrix} + \begin{bmatrix} k_1+k_2 & -k_2 & 0 & 0 \\ -k_2 & k_2 & 0 & 0 \\ 0 & 0 & 0 & 0 \\ 0 & 0 & 0 & 0 \end{bmatrix} \begin{bmatrix} \theta_2 \\ \theta_3 \\ \theta_{N1} \\ \theta_{N2} \end{bmatrix}$$
$$+ \begin{bmatrix} c_1+c_2 & -c_2 & -c_{N1} & 0 \\ -c_2 & c_2 & 0 & 0 \\ -c_{N1} & 0 & c_{N1} & 0 \\ 0 & 0 & 0 & 0 \end{bmatrix} \begin{bmatrix} \dot{\theta}_2 \\ \dot{\theta}_3 \\ \dot{\theta}_{N1} \\ \dot{\theta}_{N2} \end{bmatrix} + \begin{bmatrix} k_{N1}(\theta_2-\theta_{N1})^3 \\ 0 \\ -k_{N1}(\theta_2-\theta_{N1})^3 \\ 0 \end{bmatrix} + \begin{bmatrix} F_{kN2} \\ 0 \\ 0 \\ -F_{kN2} \end{bmatrix} = \begin{bmatrix} k_1\theta_F + c_1\dot{\theta}_F \\ -T_{RES} \\ 0 \\ 0 \end{bmatrix}$$

where

$$F_{kN2} = \begin{cases} k_{N2}(\theta_2-\theta_{N2}-e_N) + c_{N2}\left(\dot{\theta}_2-\dot{\theta}_{N2}\right) & \theta_2-\theta_{N2} \geq e_N \\ 0 & -e_N < \theta_2-\theta_{N2} < e_N \\ k_{N2}(\theta_2-\theta_{N2}+e_N) + c_{N2}\left(\dot{\theta}_2-\dot{\theta}_{N2}\right) & \theta_2-\theta_{N2} \leq -e_N \end{cases}.$$

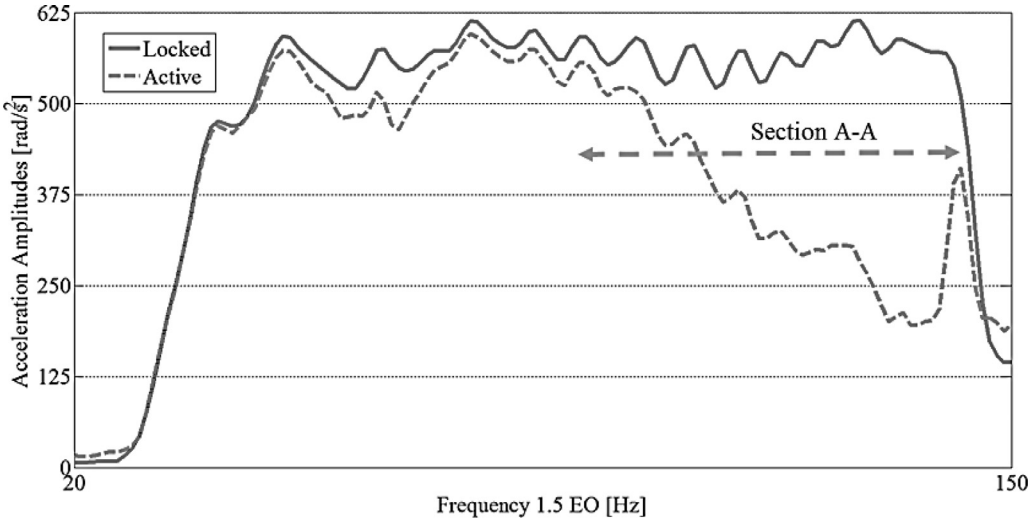

Fig. 20. Area of Effective Acceleration Amplitude Reduction for two parallel NES.

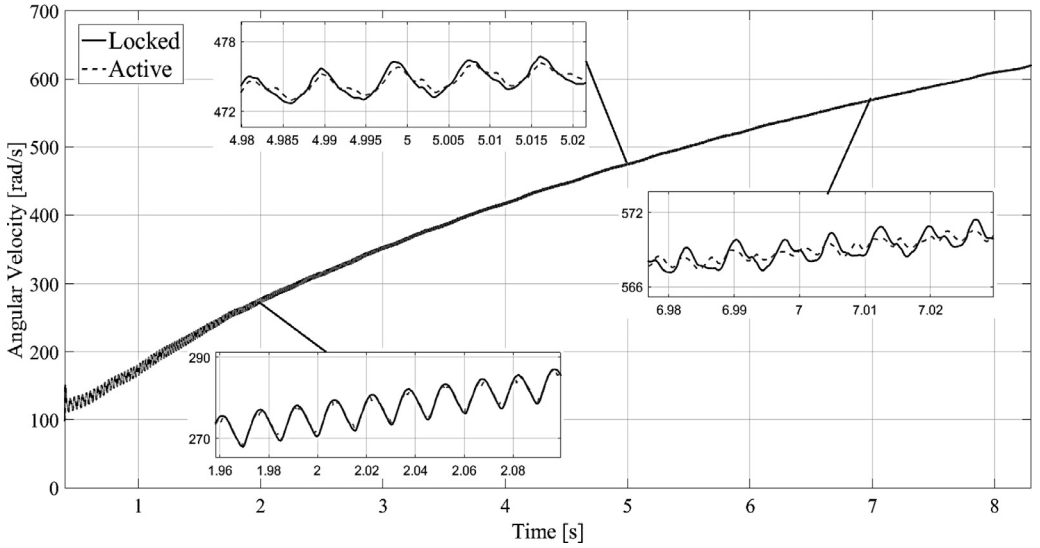

Fig. 21. Transmission Input Shaft Angular velocity for two parallel NES (vibro-impact and cubic NES) with clearance $e_N = 0.036$ rad.

From the previous single vibro-impact NES (Table 2) it was concluded that the clearance of $e_N = 0.036\ rad$ results in better attenuation of vibrations at low frequencies. Therefore, the clearance was fixed at this value. The parameters for the cubic NES are varied in the range $J_{N1} = 4 - 8\ \%$ of the transmission input shaft inertia. The parameters for the vibro-impact NES are varied in the range $J_{N2} = 8 - 12\%$ of the transmission input shaft inertia. The corresponding stiffness is changed in the range: $k_{N1} = 10^3 - 2 \times 10^9\ Nm/rad^3$ for the *cubic* NES. and $k_{N2} = 10^6 - 9 \times 10^{11}$ Nm/rad for the vibro-impact NES. The damping coefficients for both the absorbers are kept constant as: $c_{N1} = c_{N2} = 0.001$ Nms/rad. In this case the contour plots cannot be generated due to the multitude of unknown parameters. Therefore, the AEAAR is plotted against specific combinations of absorber parameters. Each combination of parameters is stored with its respective iteration number. The AEAAR plot versus iteration number is plotted in Fig. 19.

It can be concluded that the optimal parameter combinations occur at the iteration 5294, which corresponds to the parameter combination: $J_{N1} - 8\ \%$ of the transmission input shaft inertia, $J_{N2} - 8\%$ of the transmission input shaft inertia, $k_{N1} = 7.510^5\ Nm/rad^3$, $k_{N2} = 3 \times 10^{11}\ Nm/rad$, $c_{N1} = c_{N2} = 0.001$ Nms/rad with AEAAR= 13,150. The corresponding 1.5 EO harmonic acceleration amplitudes of the transmission input shaft for each optimal case are plotted in Fig. 20. The time domain gearbox input shaft velocity for the two parallel (vibro-impact and cubic) optimal NES case is plotted in Fig. 21. The cubic NES component works effectively in the high frequency range, but only small improvement is provided by the vibro-impact component at low frequencies. In fact, significant reduction in acceleration amplitudes is only obtained in the upper half of the frequency response (section A-A).

5. Conclusions and future work

In order to attenuate the severity of typical torsional oscillations present in automotive drivelines, various palliatives are implemented by automotive manufacturers (such as clutch pre-dampers, dual mass flywheels (DMFs) and DMFs with centrifugal pendulum absorbers). The above methods generally increase the weight of the driveline. The current study presents an alternative approach, using distinct types of nonlinear vibration absorbers (NES). They show the potential of suppressing oscillations over broad frequency ranges while being lightweight. These characteristics constitute their main advantages when comparing an NES with traditional vibration absorbers. Numerical analyses of the influence which different classes of NES have on reduction of torsional vibrations in an automotive drivetrain are reported. Three classes of NES analysed in this study are absorbers with: (i) cubic stiffness, (ii) fifth order stiffness, and (iii) vibro-impact NES.

A reduced two degree-of-freedom drivetrain model is used for the analyses. The model is validated in both frequency and time domains. Three different types of NES absorbers are coupled to the drivetrain model and their effect in reducing the amplitude of torsional vibrations is quantified using two criteria. The first criterion is the area of effective acceleration amplitude reduction, which indirectly quantifies the overall vibration reduction. The second criterion advises on the least attainable levels of acceleration amplitude of the transmission input shaft. A large number of simulations is carried out leading to the conclusion that for this particular application, an NES absorber with cubic stiffness can efficiently reduce the amplitude of torsional vibrations within a higher frequency range. In order to extend the performance of the NES to lower frequencies, similar analyses using NES absorbers with vibro-impacts and fifth-order nonlinearity are used. It is shown that in none of the cases considered it is possible to achieve substantial broadband vibration reduction at low frequencies. The reason for this shortcoming may be the insufficient levels of energy transmitted to the drivetrain system in order to activate the TET mechanism. The practical implication is that third-order NES should be prioritised for experimental validation of its capability to reduce vibrations in the automotive drivetrains. Furthermore, the effectiveness of utilizing more than one NES attachments acting simultaneously and tuned to different frequency regions should be examined as part of any future work.

Acknowledgment

The authors wish to express their gratitude to the EPSRC for the financial support extended to the **"Targeted energy transfer in powertrains to reduce vibration-induced energy losses"** Grant (EP/L019426/1), under which this research was carried out (research data for this paper are available on request from Stephanos Theodossiades). Thanks are also due to project partners; Ford Motor Company and Raicam Clutch for their support.

References

[1] T. Wellmann, K. Govindswamy, J. Orzechowski, S. Srinivasan, SAE Int. J. Engines 8 (2015), doi:10.4271/2015-01-2183.
[2] H. Rahnejat (Ed.), Tribology and Dynamics of Engine and Powertrain: Fundamentals, Applications and Future Trends, Woodhead Publishing, Cambridge, 2010.
[3] M. Mohammadpour, S. Theodossiades, H. Rahnejat, P. Kelly, Proc. Inst. Mech. Eng., Part K: J. Multi-Body Dyn. 228 (2013) 19–33.
[4] M. De la Cruz, S. Theodossiades, P. King, H. Rahnejat, Int. J. Powertrains 1 (2011) 137–161.
[5] H. Rahnejat, Multi-body Dynamics: Vehicles, Machines and Mechanisms, Professional Engineering Publishing, Bury St Edmunds, UK, 1998.
[6] P. Bertin, E. Breton, A. Mokdad, SAE Tech., Pap. 950893 (1995).
[7] N. Cavina, G. Serra, SAE Tech. Pap. 2004-01-3016 (2004).
[8] S. Theodossiades, M. Gnanakumarr, H. Rahnejat, P. Kelly, Proc. Inst. Mech. Eng. Part D: J. Automobile Eng. 220 (2006) 747–761.
[9] W. Sun, Y. Li, J. Huang, SAE Int. J. Passeng. Cars - Mech. Syst. 4 (2011) 1050–1057.
[10] Z. Chen, Z. Chen, Y. Mao, W. Shi, G. Zhang, SAE Tech. Pap. 2014-01-28 (2014).
[11] L.Q. Song, L.P. Zeng, S.P. Zhang, J.D. Zhou, H.E. Niu, Mech. Mach. Theory 79 (2014) 124–140.
[12] D. Chen, Y. Ma, W. Sun, X. Guo, X. Shi, in: Proceedings of the International Conference Electronic and Mechanical Engineering and Information Technology, Harbin, 2011, pp. 2706–2709.
[13] A.M. Sharaf, G. Mavros, H. Rahnejat, P.D. King, S.K. Mohan, Int. J. Heavy Veh. Syst. 15 (2008) 188–207.
[14] M. Daliri, D. Jalali-Vahid, H. Rahnejat, Proc. Inst. Mech. Eng., Part J: J. Eng. Tribol. 229 (2015) 578–596.
[15] D.E. Newland, Trans. ASME, J. Manuf. Sci. Eng 86 (1964) 257–263.
[16] C.P. Chao, C.T. Lee, S.W. Shaw, J. Sound Vib. 204 (1997) 769–794.
[17] A.S. Alsuwaiyan, S.W. Shaw, J. Sound Vib. 252 (2002) 791–815.
[18] A. Wedin, Reduction of Vibrations in Engines using Centrifugal Pendulum Vibration Absorbers, Chalmers University of Technology, 2011.
[19] A. Vakakis, O.V. Gendelman, L.A. Bergman, D.M. McFarland, G. Kerschen, Y.S. Lee, Nonlinear Targeted Energy Transfer in Mechanical and Structural Systems: Solid Mechanics and its Applications, 1st ed, Springer, 2008.
[20] D.M. McFarland, G. Kerschen, J.J. Kowtko, Y.S. Lee, L.A. Bergman, A.F. Vakakis, J. Acoust. Soc. Am. 118 (2005) 791–799.
[21] F. Nucera, A.F. Vakakis, D.M. McFarland, L.A. Bergman, G. Kerschen, Nonlinear Dyn 50 (2007) 651–677.
[22] M.A. AL-Shudeifat, A.F. Vakakis, L.A. Bergman, J. Comput. Nonlinear Dyn. 11 (2015) 021006.
[23] O. Gendelman, L.I. Manevitch, A.F. Vakakis, R. M'Closkey, J. Appl. Mech. 68 (2001) 34.
[24] A.F. Vakakis, O. Gendelman, J. Appl. Mech. 68 (2001) 42–48.
[25] A.F. Vakakis, J. Vib. Control 9 (2003) 79–93.
[26] A.F. Vakakis, L.I. Manevitch, O. Gendelman, L. Bergman, J. Sound Vib 264 (2003) 559–577.
[27] X. Jiang, D. Michael Mcfarland, L.A. Bergman, A.F. Vakakis, Nonlinear Dyn 33 (2003) 87–102.
[28] P.N. Panagopoulos, A.F. Vakakis, S. Tsakirtzis, Int. J. Solids Struct. 41 (2004) 6505–6528.
[29] S. Tsakirtzis, G. Kerschen, P.N. Panagopoulos, A.F. Vakakis, J. Sound Vib 285 (2005) 483–490.
[30] G. Kerschen, A.F. Vakakis, Y.S. Lee, D.M. McFarland, J.J. Kowtko, L.A. Bergman, Nonlinear Dyn 42 (2005) 283–303.
[31] F. Georgiadis, A.F. Vakakis, D.M. Mcfarland, L. Bergman, Int. J. Bifurc. Chaos. 15 (2005) 1989–2001.
[32] X. Jiang, A.F. Vakakis, in: Proceedings of the International Design Engineering Technical Conferences and Computers and Information in Engineering Conference, Chicago, 2003.
[33] I. Karayannis, A.F. Vakakis, F. Georgiades, Proc. Inst. Mech. Eng., Part C: J. Mech. Eng. Sci. 222 (2008) 1899–1908.

[34] R. Viguié, G. Kerschen, J.C. Golinval, D.M. McFarland, L.A. Bergman, A.F. Vakakis, et al., Mech. Syst. Signal Process. 23 (2009) 148–169.
[35] O.V. Gendelman, G. Sigalov, L.I. Manevitch, M. Mane, A.F. Vakakis, L.A. Bergman, J. Appl. Mech. 79 (2012) 011012.
[36] G. Sigalov, O.V. Gendelman, M.A. AL-Shudeifat, L.I. Manevitch, A.F. Vakakis, L.A. Bergman, Nonlinear Dyn. 69 (2012) 1693–1704.
[37] S.A. Hubbard, D.M. McFarland, L.A. Bergman, A.F. Vakakis, in: Collection of Technical Papers – AIAA/ASME/ASCE/AHS/ASC Structures, Structural Dynamics and Materials Conference, 2010, pp. 1–13.
[38] R.A. Krenz, SAE Tech. Pap. 850967 (1985).
[39] M.T. Menday, H. Rahnejat, M. Ebrahimi, Proc. Inst. Mech. Eng., Part D: J. Automobile Eng. 213 (1999) 349–357.
[40] P. Kelly, H. Rahnejat, J.W. Biermann, in: Proceedings of IMechE Conference Transaction, Mechanical Engineering Publications, 1998, pp. 167–178.
[41] M.Y. Wang, R. Manoj, W. Zhao, Proc. Inst. Mech. Eng., Part D: J. Autom. Eng. 215 (2001 p) 241–258.
[42] O. Tangasawi, S. Theodossiades, H. Rahnejat, J. Sound Vib. 308 (2007) 418–430.
[43] R. Brancati, E. Rocca, R. Russo, Proc. Inst. Mech. Eng., Part D: J. Automob. Eng. 219 (2005) 1075–1083.
[44] M. De la Cruz, S. Theodossiades, H. Rahnejat, Proc. Inst. Mech. Eng., Part K: J. Multi-Body Dyn. 224 (2010) 167–181.
[45] A. Haris, E. Motato, S. Theodossiades, A.F. Vakakis, L.A. Bergman, D.M. McFarland, et al., in: Proceedings of Conference on Dynamic System and Mathematical Numerical Approaches, 2015, pp. 245–254.
[46] A. Kooy, Solving the Powertrain Puzzle, Schaeffler Technologies GmbH & Co, Springer Fachmedien Wiesbaden, 2014, pp. 78–93.